Final Report

Task-Level Control for a Full Semi-Autonomous Mission: Test Platform Development and Demonstration

NASA Grant #NCC2-1004

Principal Investigator:
Stephen M. Rock

January 2001

Self-Calibration of Pseudolite Arrays Using Self-Differencing Transceivers

Edward A. LeMaster, *Stanford University*
Stephen M. Rock, *Stanford University*

BIOGRAPHY

Edward A. LeMaster is a Ph.D. candidate in Aeronautics and Astronautics at Stanford University. He received his B.S. in Aeronautical and Astronautical Engineering from the University of Washington in 1995 and his M.S. from Stanford in 1996. His current research focuses on developing a GPS-based pseudolite navigation system for Mars exploration. Previously, he developed an integrated GPS/computer-vision navigation system for the Stanford HUMMINGBIRD autonomous helicopter.

Stephen M. Rock is an Associate Professor of Aeronautics and Astronautics at Stanford University. He received his S.B. and S.M. in Mechanical Engineering from MIT in 1972 and Ph.D. in Applied Mechanics from Stanford University in 1978. Dr. Rock joined the Stanford faculty in 1988 where he teaches courses in dynamics and control and pursues research in developing and applying advanced control techniques for vehicle and robot applications. Prior to joining the Stanford faculty, Dr. Rock led the advanced controls group of Systems Control Technology.

ABSTRACT

Pseudolites can extend the availability of GPS-type positioning systems to a wide range of applications not possible with satellite-only GPS, including indoor and deep-space applications. Conventional GPS pseudolite arrays require that the devices be pre-calibrated through a survey of their locations, typically to sub-centimeter accuracy. This can sometimes be a difficult task, especially in remote or hazardous environments. By using the GPS signals that the pseudolites broadcast, however, it is possible to have the array self-survey its own relative locations, creating a Self-Calibrating Pseudolite Array (SCPA).

In order to provide the bi-directional ranging signals between devices necessary for array self-calibration, pseudolite transceivers must be used. The basic principles behind the use of transceivers to create an SCPA were first presented in [1]. This paper begins with a brief review of the transceiver architecture and the fundamental direct-ranging algorithm presented in that paper. This is followed by a description of a prototype self-differencing transceiver system that has been constructed, and a presentation of experimental code- and carrier-phase ranging data obtained using that system. A second algorithm is then described which uses these fundamental range measurements between transceiver pairs to self-calibrate a larger stationary array and to provide positioning information for a vehicle moving within that array. Simulation results validating the accuracy and effective convergence of this algorithm are also presented.

INTRODUCTION

The robotic exploration of other planets poses many challenges for navigation systems. Familiar terrestrial position and orientation references may be limited. Man-made landmarks such as roads do not exist, and neither do radio navigation aids such as GPS, LORAN, and VOR/DME. Moreover, the long communications time delay and limited bandwidth limit human intervention and dictate a requirement for a great deal of system autonomy.

Mars surface exploration suffers from many of these navigational challenges. The lack of a global magnetic field makes heading determination difficult without the use of star trackers. Poor traction prevents the use of odometers for long-range positioning, and rugged terrain and long-duration missions limit the use of inertial instrument packages.

These difficulties are accompanied by a growing demand for accurate and reliable navigation information. Sample-

return missions require positioning accuracy at the sub-meter level, in order to allow robots to locate and return to valuable scientific sites. As mission plans transition to more distributed systems with multiple cooperating robots, even more accurate relative positioning information is needed to enable successful completion of mission goals. This requirement also exists for potential astronaut/robot teams in the future.

GPS-type systems can greatly benefit future space exploration missions by providing centimeter-level, drift free position and degree-level attitude information to robotic explorers. GPS pseudolites allow this technology to be used in areas where satellite coverage is not yet available, or to supplement the satellites with additional ranging sources. The basic feasibility of this approach has been previously demonstrated. For example, the use of GPS pseudolite augmentation for relative positioning of formation-flying spacecraft is described in [2]-[7]. Ground-based augmentation for situations with poor satellite coverage is described in [8]-[10].

Pseudolite-only systems have also been previously demonstrated (e.g. for indoor positioning systems [11]-[13]). A similar pseudolite system, distributed on the Martian surface, would allow precise positioning of multiple robots over extended duration missions. A major difficulty with such systems, however, is in surveying the locations of the pseudolites: these must be known with an accuracy comparable to the overall navigational accuracy desired from the array. This is a significant challenge for autonomous rovers in a hostile environment. Zimmerman demonstrated that it is possible to survey in a pseudolite system using their broadcast signals by moving a receiver within the array to precisely known locations, thereby inverting the pseudolite navigation problem [13]. Although this method is infeasible for planetary exploration, the ability to have the array self-calibrate using the broadcast GPS signal is still highly desirable.

Such self-calibration is possible by collocating GPS receivers with each pseudolite transmitter, thereby creating a GPS transceiver. An array of transceivers is able to listen to the signals broadcast by each member of the array and determine the overall configuration, creating a Self-Calibrating Pseudolite Array (SCPA). Positioning to a couple of meters accuracy is possible using code-phase measurements, while centimeter-level accuracy is possible using carrier-phase measurements once the integer ambiguity is resolved. Figure 1 shows a conceptual drawing of such a system providing navigational capability to a rover on the Martian surface.
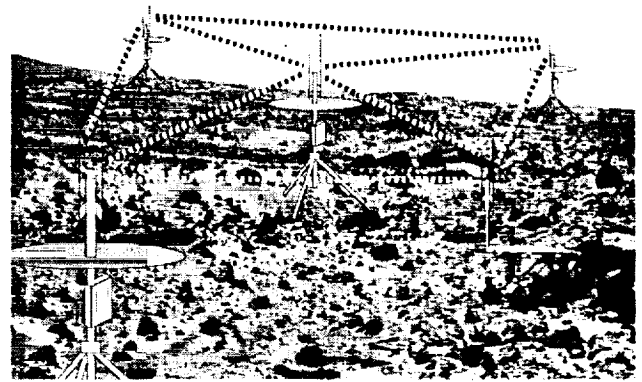

Figure 1: Mars SCPA

Although the motivation for this research is Mars exploration, SCPAs can be used in other terrestrial and space applications where the surveying of the pseudolites by other methods is difficult, impractical, or otherwise impossible. The algorithms and experimental results presented in this paper are general, and are applicable to most such applications.

TRANSCEIVER ARCHITECTURE

Transceivers can be constructed using a variety of architectures. Many of the possibilities are summarized in [14]. The architecture chosen for this project is a self-differencing transceiver, with separate transmitter and receiver components, as shown in Figure 2. This architecture was chosen for ease of construction and component integration. The output of the pseudolite is split, with one line going to a passive broadcast antenna and the other going to one front end on the dual front-end receiver. This allows the receiver to monitor the output signal, effectively measuring the relative clock bias between the pseudolite and its own receiver. The other receiver RF front end is connected to an antenna that listens for signals from other transceivers.
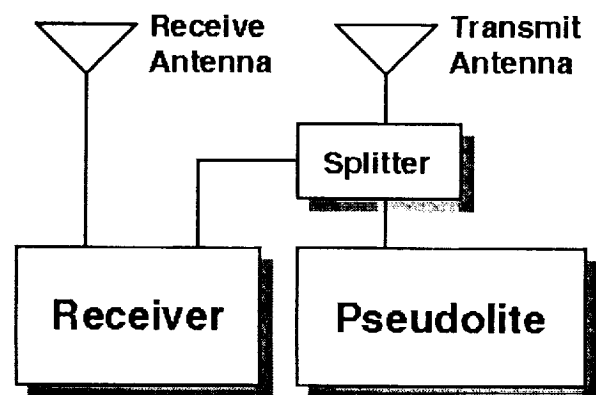

Figure 2: Transceiver Architecture

INTER-TRANSCEIVER RANGING

The simplest navigation solution using self-differencing transceivers directly determines the range between the antennas on a pair of devices, using only the signals broadcast and received by the devices themselves. This is also a very useful solution, because the ranges between any number of devices can all be solved for individually and with no changes to the fundamental equations. Figure 3 shows such a pair of devices. A description of the terminology used appears below. Note that the time biases τ_i and τ^j include common-mode effects such as transmit line biases up to the splitting point of the signal. The measurement ϕ_i^j can represent either a carrier- or code-phase measurement. In the case of carrier-phase measurements, the integers can simply be included with the line biases b_i^j, and either solved for or removed by using a-priori position information.

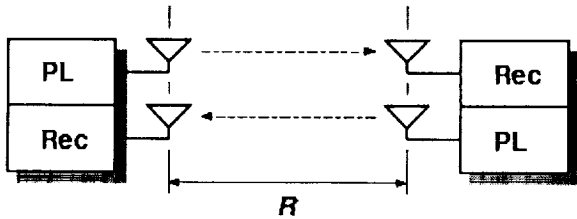|	
b_i^j	Line bias from PL j to Rec i
R_{ij}	Range between device antennas
ϕ_i^j	Rec i's measurement of PL j
τ_i	Clock bias of Rec i
τ^j	Clock bias of PL j

Figure 3: Inter-Transceiver Ranging

For this analysis it is assumed that the airborne RF pathlength between each of the two transmit/receive antenna pairs is identical and equals the range between the devices. The antenna geometry presented in Figure 3 satisfies this constraint, although other geometries may be used with slight changes to the equations. It is also assumed that the measurements are latched simultaneously. The errors associated with violating this assumption are described in [1] and [13], and can generally be made negligible over short (< 1000 km) baselines by using intelligent receiver latching strategies.

The raw measurements taken by each receiver of the signals from the two pseudolites are given in Equation 1.

$$\begin{Bmatrix} \phi_i^i \\ \phi_i^j \\ \phi_j^i \\ \phi_j^j \end{Bmatrix} = \begin{Bmatrix} b_i^i \\ b_i^j \\ b_j^i \\ b_j^j \end{Bmatrix} + \begin{Bmatrix} \tau^i \\ \tau^j \\ \tau^i \\ \tau^j \end{Bmatrix} + \begin{Bmatrix} \tau_i \\ \tau_i \\ \tau_j \\ \tau_j \end{Bmatrix} + \begin{Bmatrix} 0 \\ R_{ij} \\ 0 \\ R_{ij} \end{Bmatrix} \quad (1)$$

Eliminate any receiver clock biases or common-mode effects by taking internal single (self) differences between the signals received by a given receiver, as shown in Equation 2.

$$\Delta\phi_i \equiv \phi_i^j - \phi_i^i = \left(b_i^j - b_i^i\right) + \left(\tau^j - \tau^i\right) + R_{ij}$$
$$\Delta\phi_j \equiv \phi_j^j - \phi_j^i = \left(b_j^j - b_j^i\right) + \left(\tau^j - \tau^i\right) - R_{ij} \quad (2)$$

Combining the measurements from both receivers and inverting Equation 2, one can determine both the range between the antenna pairs and the relative clock bias of the pseudolites.

$$\begin{Bmatrix} \tau^j - \tau^i \\ R_{ij} \end{Bmatrix} = \frac{1}{2}\begin{bmatrix} 1 & 1 \\ 1 & -1 \end{bmatrix}\left\{ \begin{Bmatrix} \Delta\phi_i \\ \Delta\phi_j \end{Bmatrix} - \begin{Bmatrix} b_i^j - b_i^i \\ b_j^j - b_j^i \end{Bmatrix} \right\} \quad (3)$$

Note that unlike most conventional differencing schemes, the line biases do not cancel. This is because the signals do not travel along common lines. A similar effect occurs in multiple-antenna attitude systems. These biases must therefore be removed, either by a hardware calibration or by solving for them explicitly in the navigation algorithms.

Noise characteristics of the range measurement between a pair of transceivers are the same as for a conventional single-difference measurement, i.e. twice that of the raw receiver code- or carrier-phase measurement noise.

For very long baseline measurements (tens to thousands of km) two additional factors become important. First, as was mentioned earlier, drift in the receiver and pseudolite clocks make it difficult to latch the measurements simultaneously. This effect can be alleviated somewhat by using higher-grade oscillators. A second effect is that unlike conventional double-differencing schemes, ionospheric and troposheric delays present in terrestrial applications do not cancel. Rather, they average and add directly to the measured range.

EXPERIMENTAL SYSTEM

This section describes the prototype system used to test and validate the inter-transceiver ranging technique presented in the previous section. The GPS components of the system are two self-differencing transceivers. The pseudolite portion of each transceiver is an IntegriNautics IN200C signal generator, shown in Figure 4, broadcasting differing pseudorandom codes. These generators were chosen because of their many desirable features: programmable power levels, several different pulsing schemes, a programmable data message at variable data rates, and the ability to broadcast at frequencies offset from L1. Figure 5 shows the receiver used; a Mitel Orion receiver that has been modified to include two separate RF front ends [15]. These receivers are fully programmable, allowing the modification of the tracking loops to accommodate the pseudolite data structure. Each receiver is equipped with an RS-232 serial link for data collection.
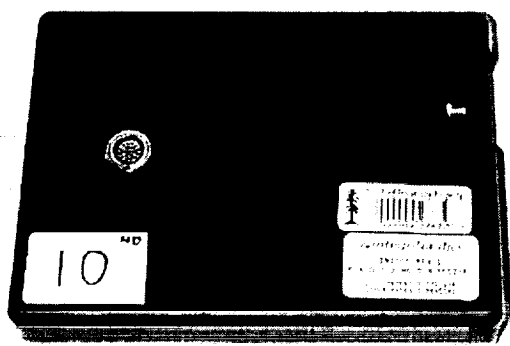

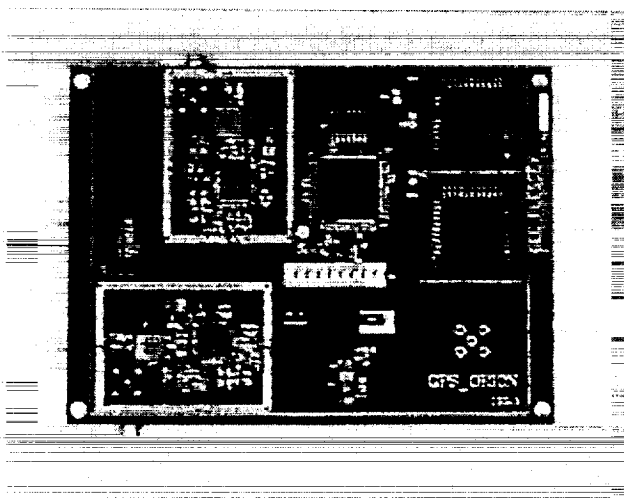Figure 4: Pseudolite Signal Generator

Figure 5: GPS Receiver

The antenna configuration used for these transceivers is shown in Figure 6. The upper black antenna is a passive patch antenna used for broadcasting the pseudolite signal, and the lower white antenna is an active patch antenna that receives signals from other transceivers. The vertical circular groundplanes help reduce multipath interference from behind the antennas and also add directionality to the antenna patterns. The horizontal groundplane between the antennas reduces the transmission between the transmit and receive antennas of the same device, helping to alleviate the near-far problem.
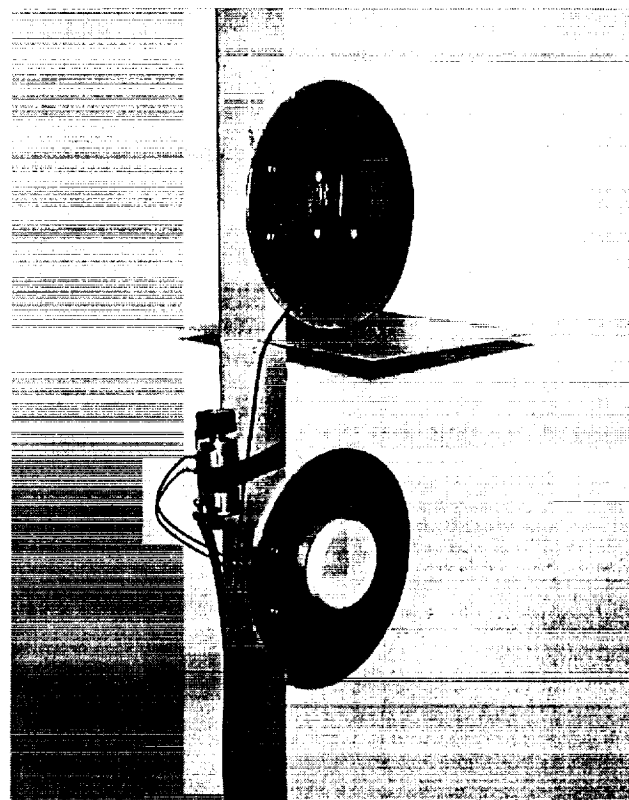

Figure 6: Antenna Configuration

Code- and carrier-phase data were collected simultaneously from both transceivers in the pair at a rate of 10 Hz, and was then post-processed to determine the range between the devices. Each data packet was time stamped by the receiver based on the current code-epoch, allowing the data to be synchronized. Missing data points were filled in by interpolation and cycle slips were removed. Real-time data processing was also performed, and showed similar performance, but did not insure synchronicity of the data or correct for missing data points.

EXPERIMENTAL RESULTS

The experimental data in this section come from a series of tests of the prototype system described above in an indoor laboratory setting. The baselines between the transceiver pair were relatively short (0.5 to 3.0 m), giving a difference in signal strength between near and far

operations of about 15.6 dB. This is smaller than the difference encountered in long-baseline operations (the collocated pseudolite is broadcasting at a very high signal strength), but allows the use of the Orion receivers without any modifications to the tracking loops. Future long-baseline (~100 m) tests are planned, following receiver modifications to allow tracking of very high SNR signals. During these tests the pseudolites were generating standard C/A signals; no pulsing was used.

The indoor test environment is a relatively cluttered room about 8 m wide and 9 m long, containing a significant amount of equipment. It therefore presents a severe multipath environment. No special efforts were taken to reduce the effect of this multipath, which is believed to be worse than the system would see in outdoor operations. Because of the excellent results obtained from the indoor system, major multipath problems are not anticipated outdoors.

Although the data collection and processing system checks for missing data points and corrects for cycle slips, these have shown themselves to be infrequent events. The receivers skip data points every 1-2 hours. Carrier-phase cycle slips occur with similar frequency for slow (<20 cm/s) relative motion between the transceivers, although they become more frequent at faster relative motions and at receiver SNRs below 10-12 dB. Code-phase cycle slips occur more frequently (several times per hour), but are correctable in a similar manner. Moreover, their large magnitude makes them easily detectable.

Figure 7 presents carrier-phase ranging data from the indoor test rig. The antennas started at a range of 3.0 m, and were then moved inward to a closest range of 0.5 m in 0.5 m increments. Truth measurements were provided by a metric scale on the floor, and are accurate to approximately 1-2 cm at antenna height. It was assumed that the initial starting separation (and thus the integer ambiguity and line biases) was known. Figure 8 shows the corresponding SNR values of the received signals in one of the two receivers, both from its own collocated pseudolite and from the other transceiver. The near-far change in SNR is clearly evident.

The ranging data show excellent tracking of the carrier-phase throughout the course of the test and through a wide range of SNR values. The mean positioning error for all of the stationary placements together was 1.29 cm, about the level of the technical error in the truth system. This includes the 4.7 cm error for the final placement, which is most likely due to operator error (the system placement is discretized at 5 cm). The other errors are due to a combination of the uncertainty in the true antenna locations and other error sources such as multipath. The ranging measurement noise level is very low, with a standard deviation of 2.3 mm.
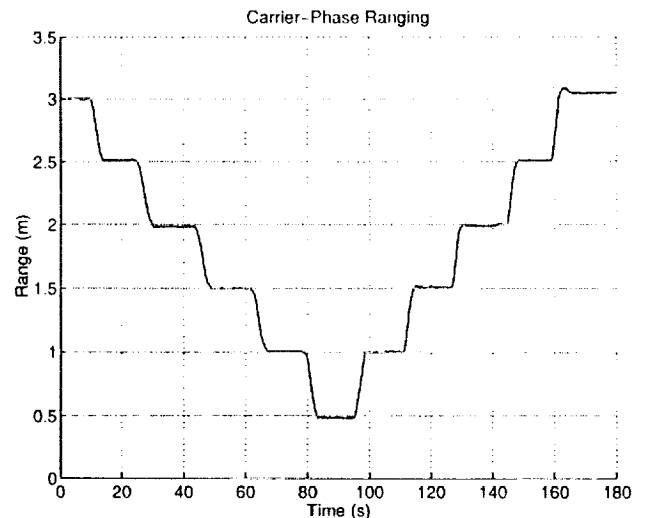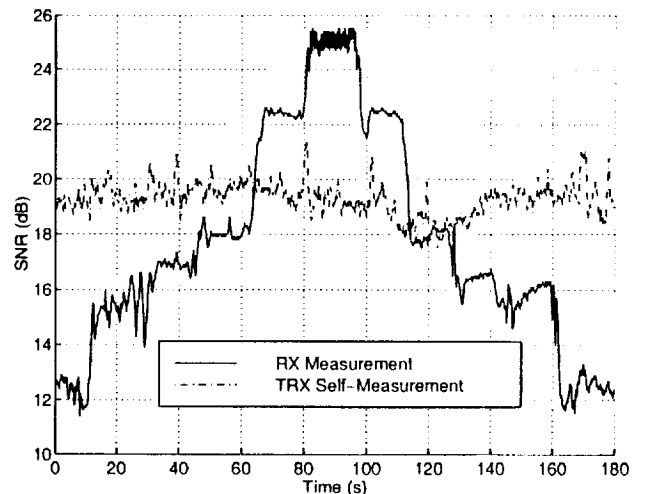

Figure 7: Carrier-Phase Data

Figure 8: Receiver SNR Values

Figure 9 shows code-phase ranging from similar test. The devices were initially separated by 3.0 m, were moved to 1.0 m, and finally back to 3.0 m. The upper plot shows the raw code-phase ranging data, while the lower shows carrier-smoothed code using a complementary filter

$$\hat{R} = \frac{a}{s+a} R_{code} + \frac{s}{s+a} R_{carrier} \qquad (4)$$

which is discretized using the bilinear transformation. The break frequency $a = 0.001 \, rad/s$ forces very close tracking of the carrier-phase data, but allows a steady-state offset due to the steady-state code-phase range estimate. The break frequency can be chosen with this low value because there is no intervening ionosphere to generate code and carrier divergence. For this plot the initial range estimate is the average value of the code-phase range over the first two minutes of data, corrected

for the line-biases estimated from another collection of data using the same hardware setup.
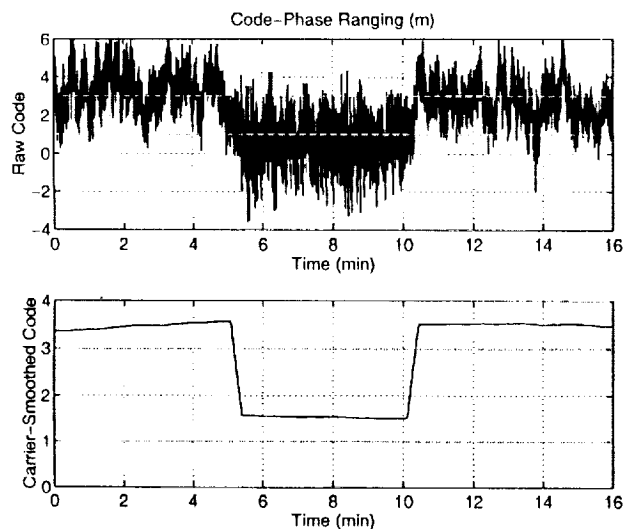
Code-Phase Ranging (m)

Figure 9: Code-Phase Data

Code-Phase Spectrum

Figure 10: Code-Phase ETFE

Although the code-phase data track the motion of the devices well, the roughly half-meter offset in the data shows the difficulty in accurately determining the code-phase line biases. Typical runs may have steady-state offsets from each other as large as 1-2 m. In addition, any given data set will see very low frequency variations of this magnitude as well. Figure 10 shows a smoothed empirical transfer-function estimate (ETFE)[16] of the frequency spectrum of 30 minutes of raw (unsmoothed) code-phase data, clearly exhibiting non-white noise characteristics with a more significant low-frequency component. This low-frequency variation is difficult to remove on a real-time basis, and the effect can be considered similar to a low-amplitude S/A-type error source. Very long averaging windows would help alleviate this problem in situations where there is no relative motion between the transceiver pairs for long periods of time.

SELF-CALIBRATION ALGORITHMS

SCPA self-calibration can be done using either code- or carrier-phase measurements. Code-phase measurements give limited (meter-level) accuracy, but have the advantage of not having an integer ambiguity. This means that once line biases have been calibrated out, a single set of static measurements serves to completely self-survey the array. For greater accuracy carrier-phase measurements are used, although this adds the aforementioned ambiguity. Motion of one of the transceivers can serve to resolve this ambiguity, and is the approach taken for the initialization algorithm presented here.
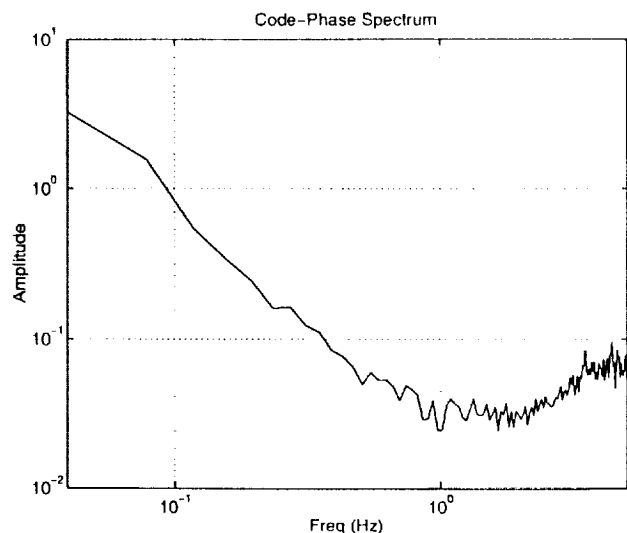
The algorithm presented in this paper differs from previous formulations because it uses the computed range between transceiver pairs – as determined using the inter-transceiver ranging technique described above – as the fundamental measurement type. It therefore presents a 2-step calculation process, first finding the $\frac{N}{2}(N-1)$ ranges between the N transceivers in the array, and then combining these range measurements to determine the array positions. Depending on the size and dimensionality of the array some of these range measurements may be redundant; these can either be incorporated using a least-squares type method, or some can simply be eliminated and ignored.

This method of using inter-transceiver ranges as an intermediate step provides several advantages over other algorithms. Recordkeeping is simplified, because all possible permutations between transmit and receive antennas do not need to be considered. Range is a fundamental physical quantity and thus makes system evaluation and diagnostics simpler, and also makes it easier to determine which measurements are redundant and can be eliminated. This greatly helps simplification when the array includes a large number of devices. Finally, the 2-step process reduces the number of unknowns that must be determined at once, offering a potential increase in algorithm speed.

Other differencing schemes involving more than two transceivers as the fundamental unit are less intuitive and more difficult to implement, but can offer potential advantages. One such advantage is the ability to use a mobile receiver on its own, instead of a full transceiver, to resolve integer ambiguities. This reduces equipment requirements at the expense of modularity and simplicity.

Because of the near-field nature of the SCPA, the problem of finding the device locations is inherently non-linear. The algorithm presented here uses standard linearized iterative least-squares to move from a poor initial estimate of array and vehicle position to a final accurate estimate. This initial estimate can be provided by direct code-phase ranging between the transceivers or through other sensors including intertial instruments and computer vision systems.

The nomenclature used in this discussion is summarized below...

$\vec{b}$	Vector of range measurement biases
$\vec{R}_n$	Range measurements at step n
$\vec{\varepsilon}_n$	Measurement errors at step n
$\vec{\rho}_n$	Vehicle position at step n
$\vec{v}$	Vector positions of static transceivers

These values at a given vehicle position are consolidated into common vectors and matrices to solve as a batch process.

$$\vec{x} \equiv \begin{bmatrix} \vec{b}^T & \vec{v}^T & \vec{\rho}_1^T & \cdots & \vec{\rho}_N^T \end{bmatrix}^T$$

$$\vec{E} \equiv \begin{bmatrix} \vec{\varepsilon}_1^T & \cdots & \vec{\varepsilon}_N^T \end{bmatrix}^T$$

$$\vec{\Psi} \equiv \begin{bmatrix} \vec{R}_1^T & \cdots & \vec{R}_N^T \end{bmatrix}^T$$

The carrier-phase measurements $\vec{\Psi}$ collected over the course of the trajectory are related to the state vector $\vec{x}$ through the non-linear relation

$$\vec{\Psi} = G(\vec{x}) + \vec{E} \qquad (5)$$

To solve this relation, it is convenient to linearize the system using small variations from the assumed state values $\vec{x}_k$.

$$\delta\vec{\Psi}_k = H_k \delta\vec{x}_k + \delta\vec{E}_k \qquad (6)$$

where

$$H_k \equiv \left. \frac{\partial G(\vec{x})}{\partial \vec{x}} \right|_{x_k}$$

$$= \left. \begin{bmatrix} -I & \frac{\partial \vec{R}_1}{\partial \vec{v}} & \frac{\partial \vec{R}_1}{\partial \vec{\rho}_1} & \cdots & 0 \\ \vdots & \vdots & \vdots & \ddots & \vdots \\ -I & \frac{\partial \vec{R}_2}{\partial \vec{v}} & 0 & \cdots & \frac{\partial \vec{R}_N}{\partial \vec{\rho}_N} \end{bmatrix} \right|_{x_k} \qquad (7)$$

Because this only approximates the non-linear relation, an iterative approach is used to descend the gradient. At each iteration step k, the solution is given by computing the left pseudoinverse H^L.

$$\delta\vec{x}_k = H^L \cdot \delta\vec{\Psi}_k = \left(H_k^T H_k \right)^T H_k \cdot \delta\vec{\Psi}_k \qquad (8)$$

where

$$\delta\vec{\Psi}_k = \vec{\Psi}_{meas} - \vec{\Psi}_k \qquad (9)$$

is the difference between the actual and expected measurement values. This provides the estimate of the state which minimizes the difference between the actual and the expected measurement values in a least-squares sense. This effectively minimizes the following cost function J_k.

$$J_k = \frac{1}{2} \left(\delta\vec{\Psi}_k - H_k \delta\vec{x}_k \right)^T \left(\delta\vec{\Psi}_k - H_k \delta\vec{x}_k \right) \qquad (10)$$

The state update equations are then

$$\begin{aligned} \vec{x}_{k+1} &= \vec{x}_k - \delta\vec{x}_k \\ \vec{\Psi}_{k+1} &= G(\vec{x}_{k+1}) \end{aligned} \qquad (11)$$

Note that in order to compute the pseudoinverse H^L one must constrain the solution. This can either be done by defining the coordinate system based on the transceiver locations and eliminating the corresponding columns of H_k, or by adding constraint equations by a technique such as Lagrange multipliers. Because of its simplicity the former method is adopted here, although it does skew the estimation error slightly towards one side of the array. One transceiver is defined to be at the origin and another is defined to lie along the x-axis. This provides the constraints necessary to make H_k full rank and invertable.

SELF-CALIBRATION SIMULATION

In order to verify that this algorithm accurately converges to the actual system states using a realistic initial estimate of transceiver locations and rover path, the following simulation was performed. The hypothetical test situation is a stationary, planar triangular array of three transceivers with 100 m separation. A fourth transceiver is mounted on a vehicle that is free to move about within the array. This is the minimum number of devices required to resolve all the observables for this case; there are no redundant measurements. It is assumed that carrier-phase measurements are being taken, and that the vehicle motion will be used to resolve both the integers and the uncalibrated line biases.

To examine the effect of geometry change on the determination of the integers and line biases, four different trajectories of the vehicle through the array were examined: a straight line through the middle of the array, a lawnmower pattern in the middle of the array, a complete circuit around the outside of the array, and a figure-eight type pattern which crosses through the array between loops around the static transceivers. These four patterns are shown in Figure 11. In each case, measurements are taken at roughly 10 m intervals.
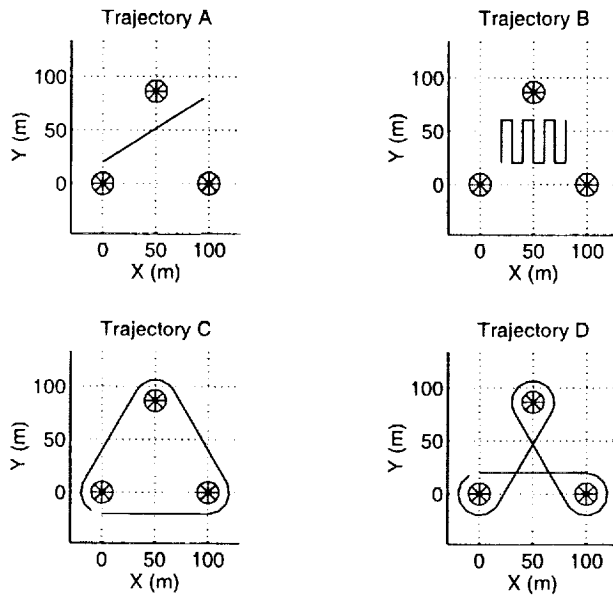

Figure 11: Sample Vehicle Trajectories

A singular value decomposition (SVD) of the pseudoinverse of the linearized geometry matrix H^L was used to evaluate the relative effectiveness of each of these trajectories. The error in the final state estimates is proportional to the measurement errors divided by the singular values σ_i.

$$\varepsilon_{state} \propto \frac{1}{\sigma_i} \cdot \varepsilon_{meas} \qquad (12)$$

Values of the minimum singular value σ_{min} for each trajectory are presented in Table 1. Singular values close to or greater than one will give centimeter-level position estimates, and are considered very good for evaluation purposes. Trajectory A performed quite poorly. Trajectory B was slightly better, but still did not provide adequate observability of all the states. Trajectories C and D both performed extremely well, with excellent observability of all states. This is because the looping around the outside of all three static transceivers. Tests show that eliminating the loop around even one transceiver can reduce the observability by a factor of 10 or greater. This is similar to the effect driving a vehicle around a pseudolite to resolve the integer ambiguities associated with CDGPS, as presented in [17].

Table 1: Minimum Singular Values for Trajectories

Trajectory	A	B	C	D
σ_{min}	0.0038	0.0172	0.6087	0.5977

Because of its excellent resolution and because it presents an interesting path, Trajectory D was used for the algorithmic simulation. The unconstrained degrees-of-freedom of the static transceivers were given a random initial estimate. The vehicle was assumed to start at a location and with a heading close to its estimated starting point, and then proceeded to attempt to follow the assigned trajectory.

Tracking errors included both random variations in the distances traveled and the steering angle and small linear drift terms in both as well. These errors are similar to those exhibited in odometers when wheel slippage occurs and when steering angles are not known precisely, and so have some level of physical plausibility. They were also chosen because they present a more difficult challenge to the algorithm, which is able to cope with spatially random initial position and trajectory estimates of up to half the size of the array. The magnitude of these error parameters, which are listed in Table 2, were chosen to give a realistic trajectory tracking accuracy which could be achievable with other non-GPS navigational sensors. In addition, unknown biases (integers and line biases) with a standard deviation of 1000 m were added to each range measurement. Measurement errors were selected to be typical of CDGPS systems, with a 1 cm standard deviation.

Table 2: Trajectory Tracking Error Parameters

	Bias	Linear Drift	Random
Distance	10 m	0.1 m/m	0.1m/m
Angle	5°	0.025°/m	0.5°/m

Figure 12 shows both the initial guess of the trajectory and transceiver locations and the final estimates. Both the trajectory and the transceiver locations converged well, giving an RMS error of 0.0074 m over the entire array. Figure 13 shows the RMS error in the estimated states as the iteration process continues. In this case, the errors fall below one centimeter RMS after 12 iterations. Bias estimate errors fall to the same order of magnitude as the other estimate errors in one iteration. Multiple simulation runs with different random trajectories show that this algorithm is reasonably robust, and performs well (80-90% successful convergence) with estimation parameter errors of twice the magnitude presented here, even though the actual trajectory at this point bears little resemblance to the initial path estimate.

Continuing algorithmic work is focused on using code-phase ranging, potentially blended with other sensor data, to provide more accurate initial estimates for the carrier-phase iteration process. Other algorithms are also being examined to attempt to reduce the sensitivity to the initial state estimate.
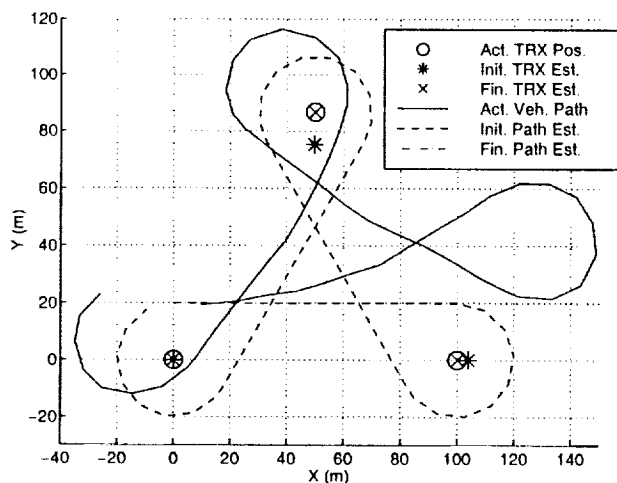

Figure 12: Self-Calibration Algorithm Results

CONCLUSIONS

This research demonstrates the potential benefits of direct ranging between transceivers for positioning applications, and demonstrates the accuracy of a self-differencing transceiver architecture for this purpose. The data presented show inter-transceiver ranging accuracy comparable to that of standard CDGPS. Of particular interest is the utilization of inter-transceiver ranging as the fundamental measurement unit for the surveying of SCPAs. The simulation shows successful array calibration from a reasonable initial state estimate, using a mobile transceiver to resolve integers. Future field tests will further validate the SCPA concept with full hardware demonstrations.
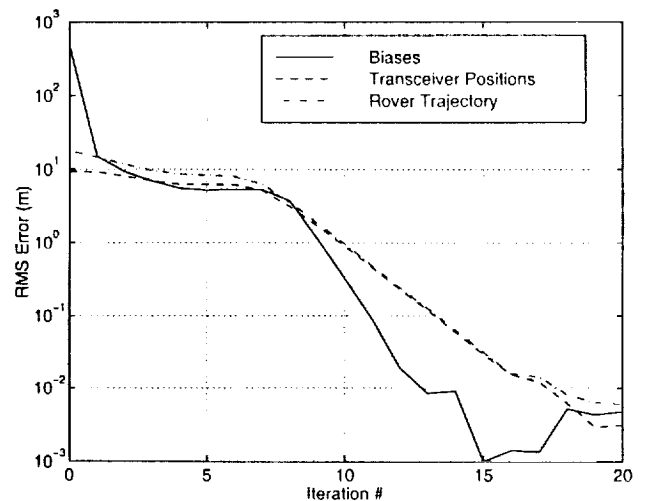

Figure 13: Self-Calibration Estimate Error

REFERENCES

[1]   LeMaster, E., Rock, S., "Mars Exploration Using Self-Calibrating Pseudolite Arrays", Proceedings of the Institute of Navigation GPS-98 Conference, Nashville, TN, Sept. 1998, pp. 1967-1974.

[2]   Corazzini, T., and How, J., "Onboard GPS Signal Augmentation for Spacecraft Formation Flying", Proceedings of the Institute of Navigation GPS-98 Conference, Nashville, TN, Sept. 1998, pp. 1937-1946.

[3]   Corazzini, Tobe', et al., "GPS Sensing for Spacecraft Formation Flying", Proceedings of the Institute of Navigation GPS-97 Conference, Kansas City, MO, Sept 1997.

[4]   Ford, Tom, et al., "HAPPI – A High Accuracy Pseudolite/GPS Position Integration", Proceedings of the Institute of Navigation GPS-97 Conference, Kansas City, MO, Sept. 1997, pp. 1719-1728.

[5] Lau, Kenneth, et al., "An Innovative Deep Space Application of GPS Technology for Formation Flying Spacecraft", In Proceedings of the AIAA GNC Conference, San Diego, CA, July 1996.

[6] Purcell, George, et al., "Autonomous Formation Flyer (AFF) Sensor Technology Development", 21st Annual AAS Guidance and Control Conference, Breckenridge, CO, Feb. 1998.

[7] Robertson, A., Corazzini, T., and How, J., "Formation Sensing and Control Technologies for a Separated Spacecraft Interferometer", American Controls Conference, Philadelphia, PA, June 1998.

[8] Altamayer, Christian, "Experiences Using Pseudolites to Augment GNSS in Urban Environments", Proceedings of the Institute of Navigation GPS-98 Conference, Nashville, TN, Sept. 1998, pp. 981-991.

[9] Holden, T., and Morley, T., "Pseudolite Augmented DGPS for Land Applications", Proceedings of the Institute of Navigation GPS-97 Conference, Kansas City, MO, Sept. 1997, pp. 1397-1404.

[10] Stone, J., and Powell, J.D., "Precise Positioning with GPS near Obstructions by Augmentation with Pseudolites", Proceedings of IEEE PLANS 1998, palm Springs, CA, pp. 562-569.

[11] Olsen, E., et al., "3D Formation Flight Using Differential Carrier-phase GPS Sensors", Proceedings of the Institute of Navigation GPS-98 Conference, Nashville, TN, Sept. 1998, pp. 1947-1956.

[12] Teague, Harris, *Flexible Structure Estimation and Control Using the Global Positioning System*, Ph.D. Thesis, Stanford University, May 1997.

[13] Zimmerman, Kurt, *Experiments in the Use of the Global Positioning System for Space Vehicle Rendezvous*, Ph.D. Thesis, Stanford University, December 1996.

[14] Stone, J., et al., "GPS Pseudolite Transceivers and their Applications", Proceedings of the 1999 Institute of Navigation National Technical Meeting, San Diego, CA, Jan. 1999.

[15] Receiver modification by Eric Olsen, Stanford University.

[16] Ljung, Lennart, System Identification: Theory for the User, P T R Prentice Hall, Englewood Cliffs, New Jersey, 1987.

[17] Elkaim, G., et al., "System Identification and Robust Control of Farm Vehicles Using CDGPS", Proceedings of the Institute of Navigation GPS-97 Conference, Kansas City, MO, Sept. 1997, pp. 1415-1424.

[18] Stengal, Robert F., Optimal Control and Estimation, Dover Publications Inc., New York, 1994.